High-resolution pulsed field ionization photoelectron-photoion coincidence spectroscopy using synchrotron radiation

G. K. Jarvis
Chemical Science Division, Lawrence Berkeley National Laboratory, Berkeley, California 94720

Karl-Michael Weitzel and Marcus Malow
Freie Universität Berlin, Institut für Physikalische und Theoretische Chemie, Takustraße 3, D-14195 Berlin, Germany

Tomas Baer
Department of Chemistry, The University of North Carolina at Chapel Hill, Chapel Hill, North Carolina 27599-3290

Y. Song and C. Y. Ng[a)]
Ames Laboratory, U.S. Department of Energy and Department of Chemistry, Iowa State University, Ames, Iowa 50011

(Received 11 June 1999; accepted for publication 1 July 1999)

We have developed a sensitive and generally applicable scheme for performing pulsed field ionization (PFI) photoelectron (PFI-PE)-photoion coincidence (PFI-PEPICO) spectroscopy using two-bunch and multibunch synchrotron radiation at the Advanced Light Source. We show that this technique provides an ion internal state (or energy) selection limited only by the PFI-PE measurement. Employing a shaped pulse for PFI and ion extraction, a resolution of 0.6 meV [full width at half maximum (FWHM)] is observed in the PFI-PEPICO bands for $Ar^+(^2P_{3/2,1/2})$. As demonstrated in the PFI-PEPICO study of the process, $O_2+h\nu\rightarrow O_2^+(b\,^4\Sigma_g^-, v^+=4, N^+)+e^- \rightarrow O^+(^4S)+O(^3P)+e^-$, the dissociation of $O_2^+(b\,^4\Sigma_g^-, v^+=4)$ in specific rotational N^+ levels can be examined. The simulation of the experimental breakdown diagram for this reaction supports the conclusion that the threshold for the formation of $O^+(^4S)+O(^3P)$ from $O_2^+(b\,^4\Sigma_g^-, v^+=4)$ lies at $N^+=9$. We have also recorded the PFI-PEPICO time-of-flight (TOF) spectra of O^+ formed in the dissociation of $O_2^+(b\,^4\Sigma_g^-, v^+=4-7)$. The simulation of these O^+ TOF spectra indicates that the PFI-PEPICO method is applicable for the determination of kinetic energy releases. Previous PFI-PE studies on O_2 suggest that a high-n O_2 Rydberg state $[O_2^*(n)]$ with a dissociative ion core undergoes prompt dissociation to yield a high-n' O-atom Rydberg state $[O^*(n')]$ [Evans *et al.*, J. Chem. Phys. **110**, 315 (1999)]. The subsequent PFI of $O^*(n')$ accounts for the formation of a PFI-PE and O^+. Since the PFI-PE intensities for O^+ and O_2^+ depend on the lifetimes of $O^*(n')$ and $O_2^*(n)$, respectively, the PFI-PE intensity enhancement observed for rotational transitions to $O_2^+(b\,^4\Sigma_g^-, v^+=4, N^+\geqslant 9)$ can be attributed to the longer lifetimes for $O^*(n')$ than those for $O_2^*(n)$. The PFI-PEPICO study of the dissociation of CH_3^+ from CH_4 also reveals the lifetime effects and dc field effects on the observed intensities for CH_3^+ and CH_4^+. The high resolution for PFI-PEPICO measurements, along with the ability to distinguish the CH_3^+ fragments due to the supersonically cooled CH_4 beam from those formed by the thermal CH_4 sample, has allowed the determination of a highly accurate dissociation threshold for CH_3^+ from CH_4. © *1999 American Institute of Physics.* [S0034-6748(99)02210-8]

I. INTRODUCTION

The study of single-photon ionization processes using mass spectrometric and photoelectron spectroscopic techniques has played an important role in providing accurate thermochemical and spectroscopic data for atomic and molecular cations.[1–5] Through appropriate energetic cycles, accurate thermochemical data for neutral species can also be obtained.[1,2] Photoelectron-photoion coincidence (PEPICO) experiments concern the detection of correlated photoelectron-photoion pairs.[6] Because of the high collection efficiency of near zero kinetic energy or threshold photoelectrons (TPEs),[7–10] the TPE detection scheme has been the preferred photoelectron spectroscopic method in the past when a tunable vacuum ultraviolet (VUV) source, such as synchrotron radiation, is used as the ionization source.[11] Hence, the coincidence scheme involving the measurement of correlated TPE-photoion pairs [referred to as the TPE-photoion coincidence (TPEPICO) method] has also been a popular technique for the study of energy- or state-selected cations.[12–14] The application of the latter method for unimolecular dissociation studies has been highly successful, providing valuable information about the dissociation threshold,

a)Author to whom correspondence should be addressed; electronic mail: CYNG@AMESLAB.GOV

dissociation rate, and kinetic energy release (KER) of fragments from parent molecular cations prepared at a well-defined internal energy or state.[12–24] Plots of the percentage abundances of reactant and product ions as a function of the parent ion internal energy (i.e., breakdown diagram) is a common method used to determine thresholds for ionic dissociation processes, from which heats of formation of fragment species can be derived.[25] The TPEPICO technique has also been successfully employed for the TPE spectroscopic measurement of a neutral cluster or a specific radical prepared in cluster or radical sources containing other impurities.[26–34] The extension of the TPEPICO technique for the detection of correlated TPEs and secondary ions formed in a collisional process, now known by the acronym of TPESICO, has been demonstrated as a powerful method for the study of state- or energy-selected ion-molecule reactions.[35–39]

The resolution and performance for all these coincidence schemes involving the TPE detection were partly limited by the hot-tail problem associated with the TPE transmission function. Recent synchrotron based studies have shown that the hot-electron problem associated with conventional TPE measurements can be greatly lessened by employing time-of-flight (TOF) discrimination in a single-bunch or a two-bunch synchrotron operation.[22,23,40] Energy resolutions for TPE measurements have typically been as good as 3–5 meV (full width at half maximum, FWHM) when electron TOF is coupled with angular discrimination against energetic or hot electrons. In these cases, the TPE resolution has been limited primarily by the monochromator optical resolution and by the incomplete TOF separation of TPEs from hot electrons.

The use of the penetrating field scheme[34,41–43] for TPE measurements has also been demonstrated to greatly reduce the hot-tail problem. We note that using the penetrating field method, along with the TOF discrimination of hot electrons, Morioka and co-workers have achieved a resolution of $\approx$1 meV (FWHM) for the TPE band of $Xe^+(^2P_{3/2})$, limited only by the obtainable optical resolution of the monochromator.[43] The successful application of the penetration field method for TPEPICO measurements have made possible the measurement of high-resolution TPE spectra for heterogeneous rare gas dimers, achieving resolutions of 2–3 meV.[34] As indicated above, this TOF discrimination method requires a single-bunch or a two-bunch synchrotron operation. At the ALS, the two-bunch mode has a light intensity more than twenty-fold lower than that provided in a multibunch synchrotron operation. We note that by nature of its design, the penetration field technique is not appropriate for accurate KER measurements.

The pulsed field ionization (PFI)-photoelectron (PFI-PE) technique[44–46] has been shown to overcome the hot-tail problem associated with TPE detection and achieve a significantly higher resolution than that of previous TPE measurements. This scheme, originally developed for using low repetition rate laser sources, has been recently demonstrated by Weitzel and Güthe in a PFI-PE study[47] of $Ar^+(^2P_{3/2,1/2})$ using single-bunch synchrotron radiation, which has a repetition rate five to six orders of magnitude greater than common laser sources.[44] In the same single-bunch experiment, they have also observed the first PFI-PE-photoion coincidence (PFI-PEPICO) band for $Ar^+(^2P_{1/2})$ despite the use of a relatively poor optical resolution of 3–5 meV (FWHM).[47]

Taking advantage of the high optical resolution made possible by the 6.65 m monochromator at the Chemical Dynamics Beam line of the Advanced Light Source (ALS), we have recently developed a novel scheme for PFI-PE measurements using monchromatized multibunch synchrotron radiation, achieving routinely resolutions of 2–5 cm^{-1} (FWHM).[48–55] Most recently, we have improved the multibunch synchrotron based PFI-PE detection scheme using an electron TOF spectrometer, demonstrating a resolution down to 1.0 cm^{-1} (FWHM) at 12.0 eV.[56] The synchrotron radiation source at the ALS has a frequency of 3.04 MHz for the two-bunch mode and in the range of 386–488 MHz for the multibunch operation and is a pseudocontinuum light source.[57] Hence, it is natural for us to further develop the PFI-PEPICO method, where parent and fragment ions are detected in coincidence with PFI-PEs. Since the ALS and most other synchrotron facilities dedicate only a small fraction of their total beam time to a single or two-bunch operation, the development of a multibunch PFI-PEPICO technique is highly desirable. The multibunch PFI-PEPICO scheme is expected to be far more sensitive because of the higher PFI-PE intensity. As discussed below, the difficulty encountered in perfecting such PFI-PEPICO experiments is similar to that in conventional TPEPICO studies. That is, the condition for good electron resolution (requires a low electric repeller field for electron extraction) is contrary to that for good ion collection efficiency (requires a high electric repeller field for ion extraction).

In this article, we discuss selected results of our recent PFI-PEPICO experiments performed at the ALS. All these PFI-PEPICO experiments take advantage of the ''dark gap'' in the two-bunch and multibunch synchrotron radiation operation. The dark gap is the part of the synchrotron ring period where no electron bunches orbit and consequently no light is emitted. The utilization of the dark gap for PFI-PE and PFI-photoion (PFI-PI) productions and extractions is an essential feature for successful PFI-PEPICO measurements.[47,49,56] For the current ALS operation, this dark gap is typically 100–150 ns at the total period of 656 ns. The methods described here represent the culmination of much experimentation in finding the best possible way to perform PFI-PEPICO measurements. The most successful scheme was first performed whilst the synchrotron was operating in the two-bunch mode whereby two 50 ps bunches of electrons separated by 328 ns make up the synchrotron ring period. The later success in multibunch PFI-PEPICO measurements using a narrower dark gap has made this technique both highly sensitive and readily applicable to the study of any molecular systems.

Results obtained on He, Ne, Ar, H_2, HCl, O_2, and CH_4 are discussed here to illustrate the performance of different PFI-PEPICO schemes. The O_2 experiment shows that breakdown diagrams can be recorded with resolutions as good as 1.0 meV. The PFI-PEPICO TOF spectra for O^+ from O_2 taken at energies corresponding to the formation of $O_2^+(b\,^4\Sigma_g^-, v^+=4-7)$ illustrate that information on KER is

preserved in the TOF spectra. By employing a shaped PFI/ion-extraction pulse, we have demonstrated in the measurement of the PFI-PEPICO bands for $Ar^+(^2P_{3/2,1/2})$ that resolutions as good as 0.6 meV (FWHM) can be achieved with excellent collection efficiencies for PFI-PE and PFI photoion (PFI-PI).

II. EXPERIMENTAL CONSIDERATIONS

The experiments were carried out at the Chemical Dynamics Beamline of the ALS associated with the Lawrence Berkeley National Laboratory.[57] Briefly, this high-resolution VUV photoionization facility consists of a 10-cm period undulator, a gas harmonic filter, a 6.65 m off-plane Eagle mounted monochromator, and a multipurpose photoelectron-photoion spectrometer.[58] All details concerning most of these elements of the Chemical Dynamics Beamline have been described in detail previously and will therefore not be elaborated upon here.

In the experiments performed here, one of two gratings, a 2400 lines/mm grating (dispersion=0.64 Å/mm) or a 4800 lines/mm (dispersion=0.32 Å/mm), was used to disperse the first harmonic of the undulator VUV beam with entrance/exit slits sizes in the range of 30–400 μm. The resulting monochromatic VUV beam was then focused into the photoionization/photoexcitation (PI/PEX) center of the photoelectron-photoion apparatus. The photon energy calibration was achieved using the $Ne^+(^2P_{3/2})$, $Ar^+(^2P_{3/2})$, $Kr^+(^2P_{3/2})$, and $Xe^+(^2P_{3/2})$ PFI-PE recorded under the same experimental conditions before and after each scan. This calibration procedure assumes that the Stark shift for ionization thresholds of the molecule of interest and the rare gases are identical. On the basis of previous experiments, the accuracy of the energy calibration is believed to within ± 0.5 meV.[48–55]

Figure 1 depicts the schematic diagram of the photoelectron-photoion coincidence spectrometer,[24] showing the lens arrangement for the electron and ion TOF detection. Here, the electrostatic lens E1–E5 and I1–I11 are associated with the electron and ion TOF spectrometers, respectively. The distance between I1 and E1 is 1.15 cm. The midpoint between I1 and E1 defines the PI/PEX center. The apertures of E1 and E4 are 6.35 and 2 mm in diameter, respectively. The electron-flight distance is 6.8 cm, which is determined by the distance between the PI/PEX center and E5. The PFI-PE detection using the electron TOF spectrometer has been described in detail in a recent publication.[56] The aperture for I1 was 10.16 cm in diameter. The ion TOF spectrometer consists of two uniform field acceleration regions and one drift region. The first uniform field region (distance=4.83 cm) is the region from the PI/PEX center to 18, while the second uniform field region (0.54 cm) is defined by the region from 18 to 19. The field free drift region comprises of the region between I9 and I11 and has a distance of 46.63 cm. Typical voltages in *V* (associated with the coincidence schemes described in Sec. II C below) applied to the electron and ion lenses and the drift region are also shown in parentheses Fig. 1. Two sets of dual microchannel plates (MCP) were used for electron and ion detection.

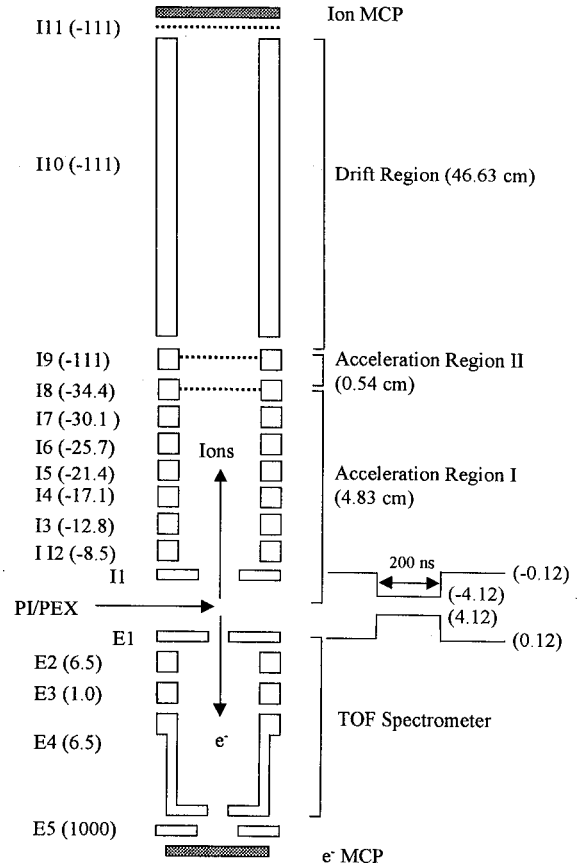

FIG. 1. Schematic diagram for the PFI-PEPICO spectrometer. The electron lenses and ion lenses are labeled as E1–E5 and I1–I11, respectively. The PI/PEX center is defined by the centered between I1 and E1. Electrons and ions are detected using MCP detectors. The ion TOF spectrometer consists of acceleration region I, acceleration region II, and a drift region with the distances of 4.83, 0.54, 46.63 cm, respectively. Typical voltages in V applied to individual lenses using the PFI-PEPICO detection scheme described in Sec. II C are given in parentheses.

The differential pumping arrangements for the photoelectron-photoion apparatus have been described in details previously.[48,49,51,58] In the present experiment, the gas sample was introduced into the PI/PEX center either as an effusive beam or a skimmed supersonic beam. An effusive beam was formed by a metal orifice with a diameter of 0.5 mm at 298 K and a distance of 0.5 cm from the PI/PEX center. A continuous molecular beam was produced by supersonic expansion from a stainless steel nozzle (diameter=0.127 mm) at a stagnation pressure of 400–600 Torr and a nozzle temperature of 298 K. For most of the beam measurements, a supersonic beam was formed by a two-stage differential pumping arrangement and was skimmed by one circular skimmer before intersecting the monochromatized VUV beam 7 cm downstream in the PI/PEX center. A supersonic beam can also be produced in a three-stage differential pumping arrangement, in which it was shaped by two skimmers. In the latter arrangement, the distance between the nozzle and PI/PEX center was $\approx$11 cm. Unless specified, the beam production system used here involves mostly the doubly differentially pumped arrangement, which provides a higher beam density at the PI/PEX center.

We describe below in chronicle order our experimenta-

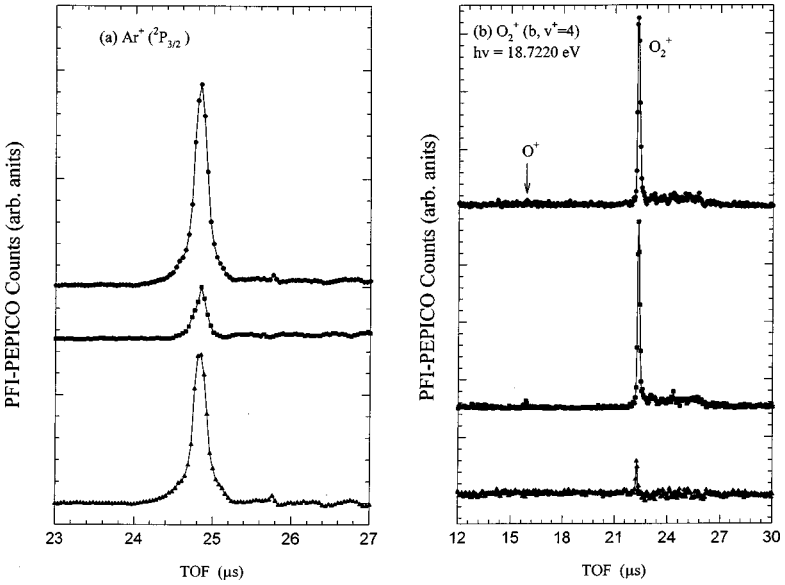

FIG. 2. PFI-PEPICO TOF spectra for (a) $Ar^+(^2P_{3/2})$ at 15.7596 eV and O_2^+ $(b\,^4\Sigma_g^-,\ v^+=4,\ N^+=1)$ at 18.7220 eV obtained using an effusive sample beam and the differential-pulsed ion extraction scheme described in Sec. II A. The second ion extraction pulse was delayed by 10 μs with respect to the first ion extraction pulse. The upper and middle TOF spectra are due to the first and second ion extraction pulses, respectively. The true PFI-PEPICO TOF spectra (bottom spectra) are the difference of the respective upper and middle spectra.

tion to find a generally applicable PFI-PEPICO scheme. The different modes of PFI-PEPICO schemes differ mostly in the method of ion extraction, i.e., the dc and pulsed electric field applied to I1 and E1. The earlier experiments reveal factors, which are important to the success of later methods. As shown by the performance of these PFI-PEPICO schemes, the ion extraction method described in Sec. II C is the most successful.

A. Differential-pulsed ion extraction scheme

In this mode of operation, the repeller plates E1 and I1 were nominally held at ground potential. An electric field pulse ($\approx$1.5 V/cm) for PFI was applied to E1 for 40 ns duration every synchrotron ring period (frequency $\approx$1.52 MHz). The application of this pulsed field was delayed by 40 ns with respect to the beginning of the 112 ns dark gap. This is the same arrangement used for PFI-PE measurements as described by Jarvis *et al.*[56] Stray electric fields from neighboring lenses push the prompt electrons created by direct photoionization and autoionization towards the electron detector leaving a window for collection of PFI-PEs generated by the PFI. Using this scheme, the PFI-PE detection was made with essentially no interference by prompt background electrons. The TOF for PFI-PEs from the PI/PEX center to the electron detector is $\approx$50 ns.

The PFI-PE signal pulse was used to trigger the application of an ion extraction field pulse (height$=-15$ V, width$=4$ μs) to I1. We estimate that the delay between the PFI-ion formation and ion extraction is $\approx$300 ns. The use of a long ion extraction pulse is designed for efficient ion collection. The PFI-PE signal pulse was also used to trigger a multichannel scaler (MCS, Stanford Research System, Model SR430) for recording the PFI-PEPICO TOF spectrum at a preset temporal interval. We note that in all MCS measurements described here, the MCS ignores other incoming PFI-PEs during this preset MCS interval.

The main drawback of this technique is that since the ion extraction pulse has a significant overlap with the VUV light bunches, uncorrelated ions formed by photoionization and PFI are also extracted toward the ion detector. These ions which are timed with the ion extraction are expected to give considerable false coincidences. A remedy is to use a double pulse scheme, whereby a second ion extraction pulse with the same height and duration as the first pulse was applied at 10 μs after the first ion extraction. This second ion extraction pulse allows the generation of a background PFI-PEPICO TOF spectrum for false coincidence correction, which can also be recorded in the same MCS scan by setting an appropriate MCS interval. By taking the difference of the spectra due to the first and second ion extraction pulses, a true PFI-PEPICO TOF can thus be obtained. This differential pulsing coincidence detection scheme has been employed in previous TPEPICO studies with good results.[26–29]

We show in Figs. 2(a) and 2(b) the PFI-PEPICO TOF spectra obtained for $Ar^+(^2P_{3/2})$ at 15.7596 eV and $O_2^+(b\,^4\Sigma_g^-,\ v^+=4, N^+=1)$ at 18.7220 eV,[51] respectively. These spectra were recorded using an effusive beam for introducing the gas sample into the PI/PEX region. The upper and middle spectra of these figures are the PFI-PEPICO TOF spectra resulted from the first and second ion extraction pulses, respectively. The bottom plots (the true coincidence spectra) are obtained by the subtraction of the middle spectra from the corresponding top spectra.

As expected, the false coincidences for $Ar^+(^2P_{3/2})$ were found to be relatively small because prompt ions cannot be formed at the PFI threshold for $Ar^+(^2P_{3/2})$. However, false coincidences for O_2^+ at 18.722 eV, which is well above the IE of O_2, prove problematic. The false coincidences due to the overlap of the ion-extraction pulse and VUV bunch are clearly discernible in Fig. 2(b). The O_2^+ peak at 21.8 μs of the middle spectrum of Fig. 2(b) results mostly from uncorrelated PFI-PIs due to the application of the second pulse. As shown in the top and middle spectra of Fig. 2(b), the uncorrelated prompt ions extracted by the ion-extraction pulses give rise to a 4 μs (the duration of the ion-extraction pulse) constant background lying in the range of $\approx$22.2–26.2 μs.

Although a true PFI-PEPICO signal for $O_2^+(b\,^4\Sigma_g^-,\ v^+$

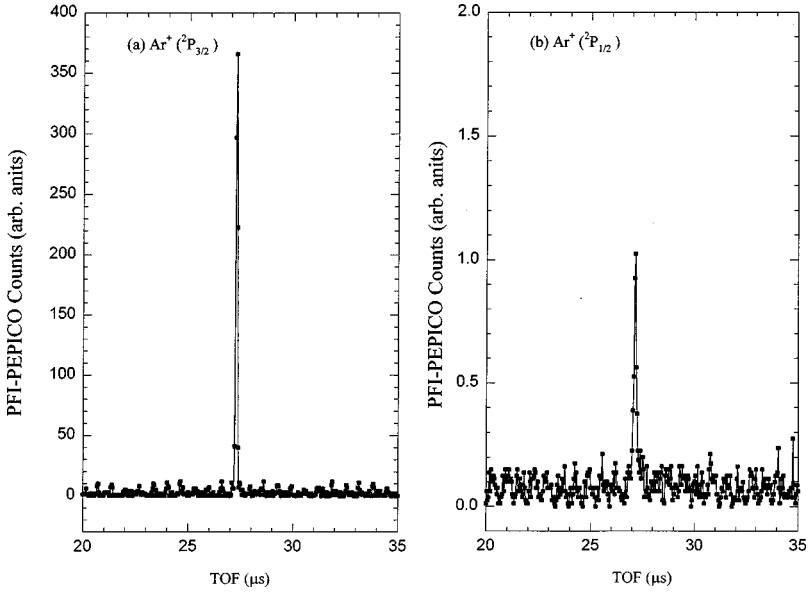

FIG. 3. PFI-PEPICO TOF spectra for (a) $Ar^+(^2P_{3/2})$ at 15.7596 eV and (b) $Ar^+(^2P_{1/2})$ at 15.9372 eV obtained using a doubly skimmed supersonic beam and the coincidence scheme described in Sec. II B. The intensities in the ordinates of these spectra are normalized to reflect the relative PFI-PEPICO signals for $Ar^+(^2P_{3/2})$ and $Ar^+(^2P_{1/2})$.

$=4$) is observed in the bottom spectrum of Fig. 2(b), the signal-to-noise (S/N) ratio is poor. The S/N ratios in the region of $\approx$22.2–26.2 μs of this bottom spectrum are also poor as a result of the subtraction. The first dissociation limit $O^+(^4S)+O(^3P)$ from O_2 is known to lie at $O_2^+(b\,^4\Sigma_g^-, v^+=4, N^+=9)$.[59–63] The energy of 18.7220 eV corresponds to the predominant production of $O_2^+(b\,^4\Sigma_g^-, v^+=4, N^+<5)$ and is expected to produce mostly O_2^+ ions. A small population of $O_2^+(b\,^4\Sigma_g^-, v^+=4, N\geqslant 9)$ associated with the *S*-branch is expected to yield a finite O^+ coincidence signal. Indeed, it is possible to see the presence of O^+ in the raw spectra. However, background subtraction negates the O^+ signal. This observation is consistent with the conclusion that the O^+ coincidence signal is too weak to be observed due the poorer S/N ratios associated with this subtraction scheme.

B. Use of a high dc field for ion extraction and a low pulse field for PFI

In this mode, a relatively high dc field is maintained at the PI/PEX region for efficient ion extraction to the ion detector. The PFI-PE TOF selection scheme was the same as described above (Sec. II A) except now that with the dc field maintained at the PI/PEX region, prompt background photoelectrons are also extracted continuously toward the electron detector. The signal pulse corresponding to the detection of a PFI-PE was used to trigger the MCS for recording the ion TOF spectrum.

Figures 3(a) and 3(b) show the PFI-PEPICO TOF spectra for the $Ar^+(^2P_{3/2})$ and $Ar^+(^2P_{1/2})$, respectively, obtained using a dc field of 8.7 V/cm at the PI/PEX region, together with an electric field pulse of 1.3 V/cm (width=40 ns) for PFI. The intensities in the ordinates of these spectra are normalized to reflect the relative PFI-PEPICO signals for $Ar^+(^2P_{3/2})$ and $Ar^+(^2P_{1/2})$. The Ar gas sample was introduced into the PI/PEX region in the form of a doubly skimmed supersonic beam produced using a triply differential pumping arrangement. The accumulation times for the PFI-PEPICO TOF spectra of Figs. 3(a) and 3(b) were 1 and 20 min, respectively. Operating the ion TOF spectrometer in space focusing conditions[64] for the dc fields, the observed coincidence $Ar^+(^2P_{3/2})$ and $Ar^+(^2P_{1/2})$ peaks are $\approx$60 ns (FWHM). The periodic spike-like structures observed in Figs. 3(a) and 3(b) are due to the false coincidences, which have a period (656 ns) identical to that of the synchrotron radiation. These false coincidence spikes result from the extraction of uncorrelated ions by the 1.3 V/cm electric pulse field intended for PFI.

By gating the Ar^+ peak intensity observed in the PFI-PEPICO TOF spectrum as a function of photon energy, we have generated the PFI-PEPICO bands for $Ar^+(^2P_{3/2})$ and $Ar^+(^2P_{1/2})$ (not shown here). As expected, these PFI-PEPICO bands are identical to the respective PFI-PE bands observed for $Ar^+(^2P_{3/2})$ and $Ar^+(^2P_{1/2})$. Using monochromator entrance/exit slits at 100/100 μm, we observed a PFI-PE and PFI-PEPICO resolution of $\approx$1 meV (FWHM).

If a sufficiently high dc electric field can be used to effectively extract ions from the PI/PEX region toward the ion detector, the use of a small pulsed electric field for PFI may not change the ion collection efficiency. This expectation is consistent with the observation that the spike-like false coincidence structures become blurred into a constant background as the dc field is increased relative to the electric pulse field for PFI. Figure 4 depicts the PFI-PEPICO TOF spectrum for H_2 observed at 15.522 eV corresponding to the $(N^+=1,\ J''=1)$ transition associated with the $H_2^+(v^+=0)$ state. This spectrum was obtained using a dc field of 15 V/cm and a pulse electric field of 1.5 V/cm. The periodic spike-like structures observed in Figs. 3(a) and 3(b) are indiscernible in Fig. 4.

We note that since PFI-PEs and PFI-PIs are only formed during the application of the pulsed field, the PFI-PIs arriving at the ion detector should correlate with the pulsed electric field. When the conditions for obtaining a PFI-PEPICO TOF spectrum such as that of Fig. 4 is fulfilled, uncorrelated prompt ions should arrive at the ion detector at a nearly uniform rate as in a dc PEPICO experiment. Thus, the ion TOF spectrum triggered by the pulsed electric field should be equivalent to a PFI-PEPICO TOF spectrum. However, by

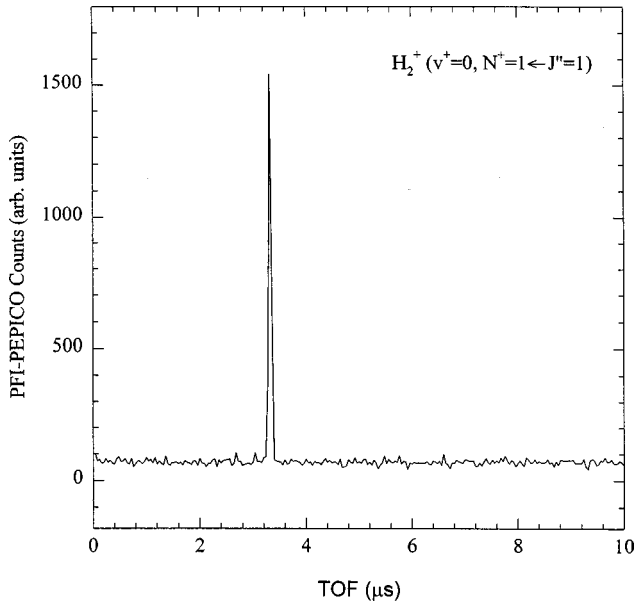

FIG. 4. PFI-PEPICO TOF spectrum for H_2^+ ($v^+=0$, $N^+=1 \leftarrow J''=1$) observed at 15.522 eV using the coincidence scheme described in Sec. II B.

recording the ion TOF spectrum only after the PFI-PE detection is expected to reduce false coincidences and thus, increase the S/N ratio of the TOF spectrum.

Another advantage of performing PFI-PEPICO using a high dc field is that it should be possible to extract kinetic energy release (KER) information from the TOF peak shape of fragment ions.[12,24] As long as the condition for space focusing is fulfilled,[64] the analysis of the TOF peak shape should resemble that of KER measurements using a conventional TPEPICO method.

However, a high dc field generally has the effect of significantly reducing the PFI-PE (or PFI-PEPICO) signal of an excited ionic state. The low intensity for $Ar^+(^2P_{1/2})$ as compared to that for $Ar^+(^2P_{3/2})$ is clearly shown in the PFI-PEPICO spectra depicted in Figs. 3(a) and 3(b). The ratio for the PFI-PEPICO intensities for $Ar^+(^2P_{1/2})$ to that for $Ar^+(^2P_{3/2})$ is $\approx$0.0025, which is nearly 200 fold lower than the expected value. The most likely reason for this is that the high dc field reduces the lifetime of the high-*n* Rydberg states converging to the excited $Ar^+(^2P_{1/2})$ states. These states can autoionize, unlike those beneath the $Ar^+(^2P_{3/2})$ peak, and are therefore far more susceptible to a field induced decay mechanism.[48] This is a major drawback of this mode of operation as excited states of other ions are expected to suffer in the same way as the $Ar^+(^2P_{1/2})$ state.

One may overcome this lifetime problem by using a lower dc field. However, the ion collection efficiency would suffer accordingly, especially in the cases where fragment ions are formed with large kinetic energy releases. The ion-extraction scheme described in Sec. II C is aimed to solve this dilemma.

C. Use of a low dc field along with a long pulse field for PFI and ion extraction

The use of a low dc field is necessary for the preservation of high-*n* Rydberg states converging to excited ionic states, i.e., the PFI-PE signal intensity. Considering that the momentum gained by an ion is proportional to the width and amplitude of the electric field pulse used, the solution to the ion-collection problem can be overcome by using a longer ion extraction pulse. This represents a compromise of the experimental scheme discussed above. We first tried this ion-extraction scheme in the two-bunch mode as the temporal interval (328 ns) between adjacent bunches is far wider than the dark gap in the multibunch mode, thus allowing the use of a wider ion-extraction pulse with no overlap of the following VUV light bunch.

In all the two-bunch experiments performed here, a dc field of 0–2 V/cm was maintained at the PI/PEX region. A 6.95 V/cm field pulse (duration=160 ns) was applied to the PI/PEX region with a delay of $\approx$100 ns with respect to each VUV light bunch. In addition to field ionizing high-*n* Rydberg states created by VUV excitation, the pulsed field also has the function of extracting the PFI ion toward the ion detector. As a result of this relatively high and wide PFI/ion-extraction pulse, we find the ion extraction to be very efficient. By comparing the coincidence rate with the PFI-PE and ion detection rates, we estimate collection efficiencies for PFI-PE and PFI-PI to be 7.3% and 19.3%, respectively, at the PFI-PE $Ar^+(^2P_{3/2})$ peak when a zero V dc field was maintained at the PI/PEX region.

TABLE I. Effect of dc electric field on the PFI-PE intensities for the $Ar^+(^2P_{3/2})$ and $Ar^+(^2P_{1/2})$ bands observed using two-bunch and multibunch synchrotron radiation at the ALS.

dc field (V/cm)	Two-bunch			Multibunch		
	PFI-PE intensity			PFI-PE intensity		
	$Ar^+(^2P_{3/2})$	$Ar^+(^2P_{1/2})$	Ratio	$Ar^+(^2P_{3/2})$	$Ar^+(^2P_{1/2})$	Ratio
0.000	0.806	0.124	0.154	1.050	0.714	0.680
0.210	⋯	⋯	⋯	1.010	0.596	0.590
0.870	1.000	0.294	0.294	1.000	0.230	0.230
1.304	⋯	⋯	⋯	0.950	0.209	0.220
1.739	0.896	0.411	0.459	0.870	0.130	0.149
2.609	0.788	0.028	0.035	⋯	⋯	⋯
3.478	0.736	0.010	0.014	⋯	⋯	⋯
5.217	0.637	0.004	0.007	⋯	⋯	⋯
6.261	0.527	0.003	0.007	⋯	⋯	⋯

It was discovered that a small dc field enhances the PFI-PE signal level of the spin-orbit excited $Ar^+(^2P_{1/2})$ states. Table I shows the relative PFI-PE intensities for $Ar^+(^2P_{3/2})$ and $Ar^+(^2P_{1/2})$ observed at different dc fields, while keeping the same ion extraction pulse field (height=6.95 V/cm, width=160 ns). The PFI-PE intensity for $Ar^+(^2P_{3/2})$ changes very little, whereas the $Ar^+(^2P_{1/2})$ PFI-PE intensity varies dramatically. The optimum voltage for these two-bunch experiments was found to be at 1.74 V/cm. This enhancement is most likely caused by lifetime lengthening of high-n Rydberg states converging to the $Ar^+(^2P_{1/2})$ ionization limit due to the Stark field and ion induced l and m_l mixing, where l is the angular momentum quantum number and m_l is the magnetic quantum number.[65–67] At larger l orbitals, the electron no longer penetrates the ion core and these states become very long lived. A low electric field is known to promote the decay of very high-n Rydberg states by field ionization, but at the same time has a lifetime lengthening effect for relatively low-n Rydberg states by l mixing.[65,67]

While operating with multibunch synchrotron radiation, a different situation arises whereby dc fields <0.2 V/cm are found to give the highest PFI-PE signal level for $Ar^+(^2P_{1/2})$ (see Table I). The difference may be caused by the fact that in the two-bunch mode, a significantly higher ion density is formed. Each bunch is filled to a maximum current of 25 mA in the two-bunch mode, as compared to that of 1.5 mA in the multibunch operation. Thus, the ion density produced in the two-bunch mode is $\approx$17-fold higher than that resulted in the multibunch operation. An inhomogeneous electric field arisen from photoions thus produced adjacent to high-n Rydberg species has been ascribed to induce m_l mixing, creating longer lived high-n Rydberg states.[65] Without this higher ion number density in the multibunch mode, m_l mixing is expected to be more subdued. However, this scenario seems unlikely as ion count rates indicate no more than one ion per electron bunch was present in the interaction region at any one time.

A second possibility is that the electric field may promote l mixing and its prolonged use may also reduce the lifetime of Rydberg species formed from photoexcitation. In other words, l mixing may occur in the picosecond time frame, which is then followed by a decay mechanism that takes place on a nanosecond time frame. In the two-bunch case, PFI takes place at most 100 ns after excitation. In the multibunch case, those excited Rydberg states formed in the first part of the multibunch cycle are not field ionized until 400 ns later. If these states are then detrimentally affected by the dc field, even after mixing, then the overall effect in total signal in the multibunch case may be a decrease. We found that the dc electric fields employed in the two-bunch and multibunch modes have similar effects on PFI-PE intensities of other atoms and molecules compared to that for the $Ar^+(^2P_{1/2})$ PFI-PI peak.

A further point of note is that a small transverse dc field ($\approx$0.5 V/cm) was also found to be advantageous to the signal levels as observed in the PFI-PE intensity for $Ar^+(^2P_{1/2})$, which increases by about 10% with the transverse field on. This again is most likely induced by m_l mixing due to the existence of this transverse or noncylindrical electric field.[65,67]

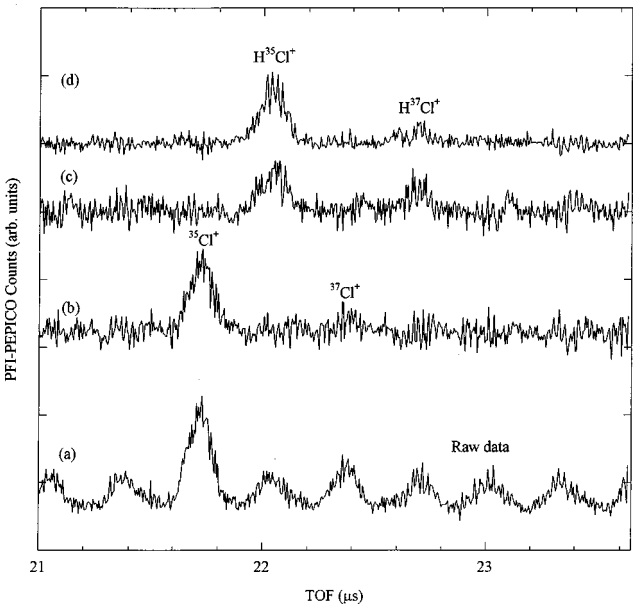

FIG. 5. (a) Raw PFI-PEPICO TOF spectrum for Cl^+ from HCl at 17.4000 eV [$HCl^+(v^+=7)$]. (b) Background subtracted PFI-PEPICO spectrum for Cl^+ from HCl at 17.4000 eV [$HCl^+(v^+=7)$]. (c) Background subtracted PFI-PEPICO TOF spectrum for Cl^+ and HCl^+ from HCl at 17.1249 eV [$HCl^+(v^+=6)$]. (d) Background subtracted PFI-PEPICO TOF spectrum for Cl^+ and HCl^+ from HCl at 16.9712 eV [$HCl^+(v^+=5)$]. These spectra were recorded in the two-bunch mode using a HCl supersonic molecular beam and the coincidence scheme described in Sec. II C.

In the multibunch experiments described under this section, a dark gap of 144 ns was available in an ALS synchrotron period. A dc field of 0.20 V/cm was applied across the PI/PEX region. The application of a PFI-extraction electric field pulse (height=6.96 V/cm, width=200 ns) was delayed by $\approx$10 ns with respect to the beginning of the 144 ns dark gap. The employment of a lower dc field makes it necessary to use a pulse with a longer duration (200 ns) than the dark gap. The overlap of 134 ns between the pulsed field and the dark gap should not produce any prompt electron and ion backgrounds. Of course, by overlapping the pulsed field with the light bunches, the pulsed field will field ionize the first set of light bunches of 66 ns measured with respect to the end of the dark gap. Any Rydberg states formed in this overlap region of 66 ns should be depleted by PFI. However, background prompt ions and PFI-PEs produced within this period may not be efficiently extracted because the momentum gained by an ion in such a pulsed field for $<$66 ns is inadequate for its transmission to the ion detector. An overlap of $<$66 ns was found to have little effect on the multibunch PFI-PE measurement. The field that all ions see is pseudo-continuous with the consequence that false coincidences arrive at the ion detector with a time structure that depends on the ring period, or rather the electric pulse field frequency. True coincidences measured relative to the observed PFI-PEs arrive at a fixed time on top of this structured background.

Figure 5(a) depicts the PFI-PEPICO TOF spectrum for Cl^+ formed from HCl at 17.400 eV, corresponding to the

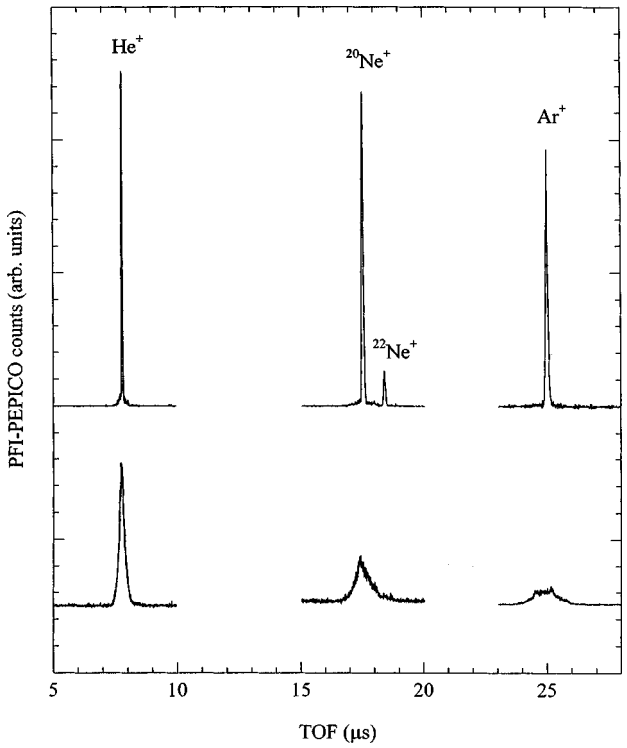

FIG. 6. PFI-PEPICO TOF spectra for $He^+(^2S_{1/2})$, $Ne^+(^2P_{3/2})$, and $Ar^+(^2P_{3/2})$ obtained at the multibunch operation using the molecular beam (upper spectra, sharp peaks) and effusive beam (lower spectra, broad peaks) arrangements. The spectra were recorded by employing the coincidence scheme described in Sec. II C and were background subtracted. The simulation of the sharp molecular beam PFI-PEPICO TOF peaks reveals a contribution of ≈15% thermal background.

initial formation of $HCl^+(X, v^+=7)$, which is just above the dissociation threshold for Cl^+.[68] This spectrum was recorded while operating in the two-bunch mode with wide monochromator entrance/exit slits of 400/400 μm. Due to the high signal level, the false coincidences are high and have a time structure with a period identical to that of the synchrotron ring. Minimizing the signal level by narrowing the slits or by reducing the molecular beam pressure greatly reduces the periodic false coincidence background. However, even without doing this, the oscillatory background can be easily subtracted. By averaging over the first and latter part of the scans to form a background for each 656 ns block of the scan and by duplicating the averaged sections together, a full background spectrum was obtained. The subtraction of the background spectrum from the spectrum of Fig. 5(a) yields the true PFI-PEPICO spectrum shown in Fig. 5(b), which is relative free from the oscillatory false coincidence background and reveals the $^{35}Cl^+$ and $^{37}Cl^+$ fragment ion peaks. The background subtracted PFI-PEPICO spectra for HCl^+ from HCl at energies (17.1249 and 16.9712 eV) corresponding to the formation of $HCl^+(X, v^+=5 \text{ and } 6)$ are also plotted in Figs. 5(c) and 5(d), respectively. In these spectra, the parent $H^{35}Cl^+$ and $H^{37}Cl^+$ ion peaks are discernible. Recently, the state selective predissociation spectra of $HCl^+(X\,^2\Sigma^+, v^+=6,7,8)$ have been reported by Penno *et al.*[68] The current date confirm that the $v^+=6$ state lies below the thermochemical limit for Cl^+ formation.

Figure 6 compares the PFI-PEPICO TOF spectra for $He^+(^2S_{1/2})$, $Ne^+(^2P_{3/2})$, and $Ar^+(^2P_{3/2})$ obtained at the multibunch operation using the molecular beam (upper spectra) and effusive beam (lower spectra) arrangements, respectively. We note that TOF peaks due to both the $^{20}Ne^+(^2P_{3/2})$ and $^{22}Ne^+(^2P_{3/2})$ isotopes are observed in Fig. 6. The narrower TOF peaks for $He^+(^2S_{1/2})$, $Ne^+(^2P_{3/2})$, and $Ar^+(^2P_{3/2})$ are due to the low translational temperature (≈20 K) in the direction the ion TOF axis (or perpendicular to the molecular beam) achieved in the molecular beam production arrangement. The significantly greater TOF peak widths observed in the effusive beam experiment is consistent with the higher translational temperature (298 K). In addition to giving rise a periodic background structure, the pulsed ion-extraction field also affects the TOF peak shape of the coincident ions. This is particularly apparent for the broad $Ar^+(^2P_{3/2})$ ion peak observed using the thermal samples (see Fig. 6). The simulation of the molecular beam PFI-PEPICO TOF peaks for the rare gas ions shown in Fig. 6 reveals the contribution of ≈15% thermal background, resulting from photoionization of random background gases in the PI/PEX region. This background depends on the photoionization chamber pressure, which was in the low 10^{-5} Torr range during the experiment. Considering that the estimated number density of the supersonic beam at the PI/PEX center is in the 10^{-4} range, the finding of a 15% thermal background is thus reasonable.

As expected, the pulsed ion extraction has little effect on the relative TOF of ions arriving at the detector. A plot (not shown here) of the TOF of rare gas ions versus the square root of the mass for He^+, Ne^+, Kr^+, Ar^+, and Xe^+ reveals a linear relationship as is normally observed for a static field extraction. We also found that the ion collection efficiency decreases as the ion mass is increased. This can be easily understood by the fact that for the same momentum gained by ions in a pulsed extraction arrangement, the heavier ion gains a lower velocity component toward the ion detector and thus has a lower ion transmission factor. The relative MCP detection efficiencies for ions with different masses may also play a role. The ion collection efficiencies are also found to be poorer for the effusive than for the molecular beam samples. In an effusive beam experiment, the interaction volume for the VUV beam and gas beam is significantly larger than that in the molecular beam arrangement, resulting in a higher signal for PFI-PE and ion detection. However, the ion transmission factor is expected to be very poor for ions formed at a large distance from the ion TOF axis.

III. RESULTS

Since the PFI and ion-extraction scheme described in Sec. II C is the most successful, the experimental results presented below are obtained using such a scheme. As indicated above, we first learned about the important experimental conditions of PFI-PEPICO measurements in the two-bunch experiments. The multibunch measurements provide a higher signal level, but the experimental conditions are more restrictive. Using O_2 and CH_4 as the molecular samples, the results presented below illustrate the performance of this PFI-PEPICO method in the internal state or energy selection of

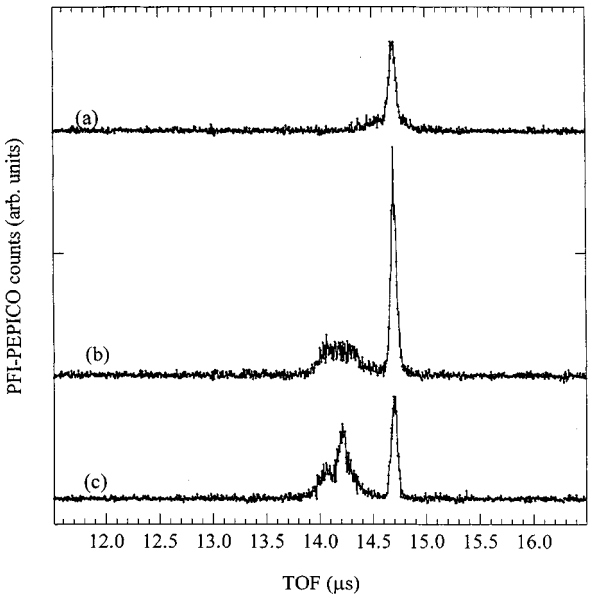

FIG. 7. Background subtracted PFI-PEPICO TOF spectra for CH_3^+ and CH_4^+ from CH_4 at (a) 14.118 eV, (b) 14.304 eV, and (c) 14.318 eV, respectively, obtained using a supersonically cooled CH_4 beam and the coincidence scheme described in Sec. II C.

ions, breakdown diagram determination, and KER measurement. Some important considerations concerning Rydberg state lifetime effects on PFI-PEPICO measurements of breakdown diagram for state- or energy-selected unimolecular dissociation processes are also discussed.

A. PFI-PEPICO study of CH_4

We have obtained detailed PFI-PEPICO TOF spectra for CH_3^+ from CH_4 near the dissociation threshold. The bulk of the data for CH_4 including important thermochemistry will be presented in a later publication. However, some of the data are presented here to illustrate factors that need to be considered when performing PFI-PEPICO experiments, especially in the measurement of accurate ion dissociation thresholds.

A most serious difficulty in the determination of ion dissociation thresholds involving a polyatomic parent species is the hot band effect.[1] Thermal populations of the parent molecules can lead to ion dissociation at energies well below the 0 K thermochemical onset. Even when a cold supersonic beam is used, the thermal contribution due to background molecules in the photoionization chamber can give rise to ambiguity in the determination of the true ion dissociation threshold. We show in Figs. 7(a)–7(c) the PFI-PEPICO TOF spectra for CH_3^+ and CH_4^+ from CH_4 at 14.118, 14.304, and 14.318 eV, respectively, obtained using a MCS channel width of 5 ns. The dissociation threshold is known to occur at 14.323 eV at 0 K.[2] Figure 7(b) reveals a narrow TOF peak for CH_4^+ and a broad TOF peak for CH_3^+. The narrow CH_4^+ peak indicates that the CH_4^+ ions are formed predominantly from photoionization of the supersonically cooled CH_4 sample, whereas the broad CH_3^+ peak is produced exclusively by the dissociative PFI of thermal (298 K) CH_4 in the photoionization chamber. Interestingly, the broad peaks seen in the TOF spectra seem to account for far more of the total signal than they should do at energies approaching threshold. Well below threshold, only a small portion of the CH_4^+ peak ($\approx$15%) is seen to originate from the thermal CH_4 [see Fig. 7(a)], but at 14.318 eV, the broad CH_3^+ part accounts for close to 50% of the total signal.

In the present PFI-PEPICO study of CH_3^+ from CH_4, the formation of CH_3^+ and CH_4^+ near the dissociation threshold can proceed by two mechanisms.

$$CH_4 + h\nu \rightarrow CH_4^*(n) \rightarrow CH_4^{*+} + e^- \rightarrow CH_3^+ + H + e^- \quad (1)$$

and

$$CH_4 + h\nu \rightarrow CH_4^*(n) \rightarrow CH_3^*(n') + H \rightarrow CH_5^+ + e^- + H, \quad (2)$$

where the $CH_4^*(n)[CH_3^*(n')]$ is the neutral excited $CH_4[CH_3]$ in a high-n [high-n'] Rydberg state. According to mechanism (1), $CH_4^*(n)$ prepared in VUV photoexcitation is first field ionized to produce internally excited CH_4^{*+} prior to dissociation forming $CH_3^+ + H$. Here, CH_4^{*+} represents the ionization limit or the ion core of $CH_4^*(n)$. In mechanism (2), $CH_4^*(n)$ first undergoes prompt dissociation to form $CH_3^*(n') + H$. The subsequent PFI of $CH_3^*(n')$ results in the formation of $CH_3^+ + e^-$.

The recent lifetime measurements for $O_2^*(n)$ converging to dissociative O_2^+ states[51,54,55,58] provide strong support for mechanism (2) as the major process for CH_3^+ formed in the PFI of $CH_4^*(n)$. The higher than expected PFI-PEPICO intensity for CH_3^+ from thermal CH_4 observed below the dissociation threshold can be accounted for by a longer lifetime for $CH_3^*(n')$ than that for $CH_4^*(n)$. As the $CH_3^*(n')$ channel becomes available, a greater PFI-PE efficiency is thus expected. The latter expectation was confirmed in the PFI-PE measurement of CH_4.[68] Since the (15%) thermal sample has a large distribution of energies, as the dissociation threshold is approached, the formation of CH_3^+ from $CH_3^*(n')$ will be favored for the thermal CH_4 sample over CH_4^+ from the supersonically cooled CH_4 sample.

Due to the magnification of the CH_3^+ intensity from thermal CH_4, the breakdown diagram will reveal a lower cross over point if CH_3^+ ions from both thermal and cold CH_4 are included in the data analysis. One important conclusion from this analysis is that we can significantly reduce this effect by constructing the breakdown diagram using only the intensity of CH_3^+ from the cooled molecular beam CH_4 sample. Although any molecular beam will have a thermal contribution from background molecules in the photoionization chamber, the CH_3^+ TOF peaks resulting from the thermal and molecular beam parts of the sample have different widths [see Fig. 7(c)] and can be easily distinguished. By analyzing the narrow part of the spectrum to obtain the ''cold'' breakdown curve, we have obtained a highly accurate value for the CH_3^+ dissociation threshold.[68] Although the lifetime effect may still play a role in the cold molecular beam sample, the effect should only occur over a narrower energy range.

It was also found that the magnitude of the dc field applied in the PFI-PEPICO experiment has an effect on the breakdown diagram determination. Figures 8(a) and 8(b) show the PFI-PEPICO TOF recorded at dc fields of 1.32 and 0 V/cm, respectively, for CH_4 at 14.309 eV. All experimental

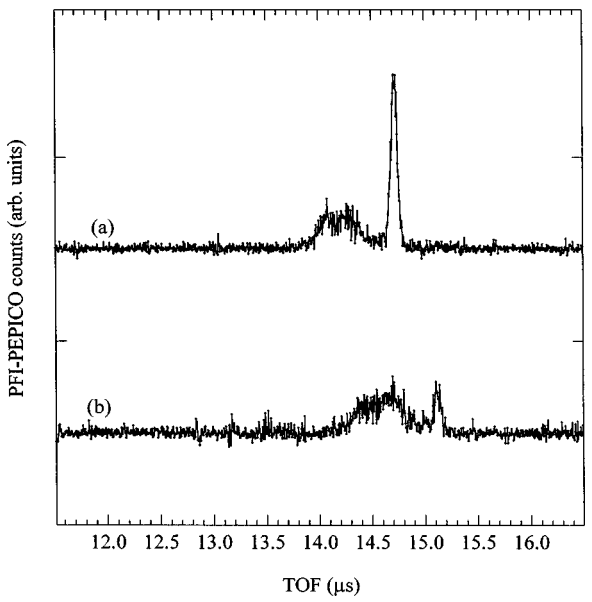

FIG. 8. Background corrected PFI-PEPICO TOF spectra recorded at (a) 1.32 and (b) 0 V/cm for CH_4 at 14.309 eV obtained using a supersonically cooled CH_4 beam and the coincidence scheme described in Sec. II C.

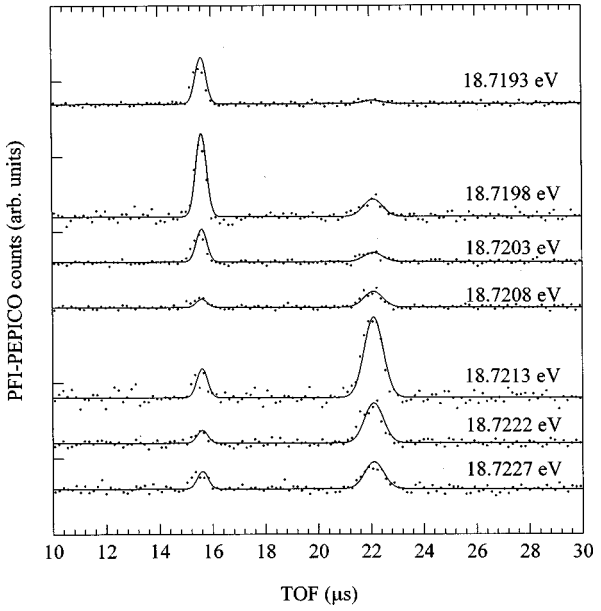

FIG. 9. Background subtracted PFI-PEPICO TOF spectra for O^+ and O_2^+ from O_2 at 18.7193–18.7227 eV obtained using an effusive O_2 beam and the coincidence scheme described in Sec. II C.

conditions except the dc field were kept constant. These spectra were recorded with an optical resolution of roughly 4 meV (FWHM). The small change in energy due to the stark shift should have little consequence on the spectrum recorded. However, as can be seen, the relative intensities of the CH_3^+ and CH_4^+ peaks change dramatically. It seems that l mixing caused by the dc electric field plays a role in lengthening the lifetime of $CH_4^*(n)$ compared to $CH_3^*(n')$. This dramatic dc Stark field effect observed on the PFI-PE intensities of CH_3^+ and CH_4^+ indicates that the patterns of low-n Rydberg states for CH_3 and CH_4 near the dissociation threshold are different, resulting in different dc field dependencies for the PFI-PE intensities for CH_3^+ and CH_4^+. This effect should be general for most molecules and may give rise to irregular structure of the experimental breakdown diagram based on PFI-PEPICO TOF measurements.

These findings indicate that for a PFI-PEPICO study of a polyatomic molecule, where individual vibrational and rotational states are not identifiable, the use of a sample containing a large thermal fraction may lead to a breakdown diagram with finite irregularities in the branching ratio profiles. The analysis and interpretation of such branching ratio data for the determination of 0 K ion dissociation thresholds involving polyatomic molecules will be discussed in fore coming publications.[69,70]

B. PFI-PEPICO study of O_2

We have performed PFI-PEPICO TOF measurements using both two-bunch and multibunch synchrotron radiation, obtaining the breakdown diagram for $O^+(^4S)+O(^3P)$ from $O_2^+(b\,^4\Sigma_g^-, v^+=4, N^+)$. The dissociation threshold is known to occur just below $O_2^+(b\,^4\Sigma_g^-, v^+=4, N^+=9)$.[64–67] The two-bunch mode measurements were made using the O_2 molecular beam sample, achieving a rotational temperature of ≈10 K, which is too low to promote a significant population for $N''=9$. Since the thermal O_2 sample promotes the populations of $N^+ \geqslant 9$, which are responsible for the observed O^+ fragment ions in the PFI-PEPICO measurements, we have examined in detail the branching ratios for O^+ and O_2^+ from O_2 in a multibunch PFI-PEPICO TOF experiment using an effusive O_2 sample. We have obtained PFI-PEPICO TOF spectra in the energy region of 18.7129–18.7253 eV at an energy increment of 0.5 meV. Selected TOF spectra measured at photon energies of 18.7193–18.7227 eV are depicted in Fig. 9. The resulting breakdown diagram can be seen in Fig. 10(a), where the solid circles represent the branching ratios of O^+ and the solid squares are those for O_2^+. At a given photon energy in the breakdown diagram, the sum of the branching ratios for O^+ and O_2^+ is normalized to 100.

In order to simulate of the breakdown diagram, it is necessary to find the rotational population of $O_2^+(b\,^4\Sigma_g^-, v^+=4)$. For this reason, we have recorded the PFI-PE band for $O_2^+(b\,^4\Sigma_g^-, v^+=4)$ [open circles shown in Fig. 10(b)] employing monochromator entrance/exit slits of 30/30 μm, together with the simulation based on the Buckingham–Orr–Sichel (BOS) model. The marking of the $\Delta N=N^+-N''=-2$, 0, and +2 (or *O*, *Q*, and *S*, respectively) rotational branches are also shown in Fig. 10(b). Here N^+ and N'' are the rotational quantum numbers for O_2^+ and O_2, respectively. We note that the numbers given in Fig. 10(b) are N'' values. The BOS simulation of this spectrum was made using the known rotational constants for $O_2(X\,^3\Sigma_g^-, v''=0)$ and $O_2^+(b\,^4\Sigma_g^-, v^+=4)$, the IE value for the formation of $O_2^+(b\,^4\Sigma_g^-, v^+=4)$, and BOS coefficients (C_0, C_2) were set at (0.3, 0.7) as determined previously by Hsu *et al.*[53] Similar to the previous study, the initial BOS fit was relatively poor in the region of 18.717–18.722 eV. An excellent fit [solid line shown in Fig. 10(a)] to the experimental PFI-PE spectrum was only observed after scaling the BOS line strengths

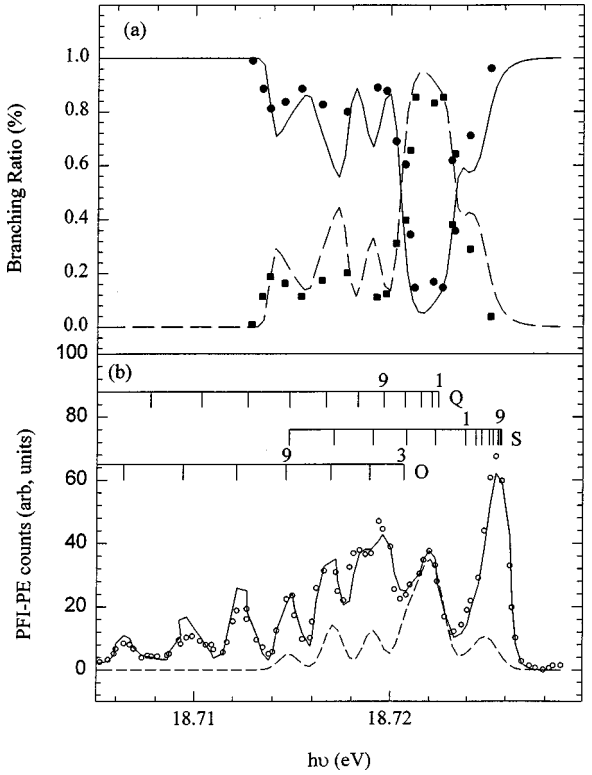

FIG. 10. (a) Breakdown diagram for the formation of $O^+(^4S)+O(^3P)$ from O_2 in the energy range of 18.705–18.730 eV. The solid circles represent the branching ratios of O^+ and the solid squares are those for O_2^+. At a given photon energy, the sum of the branching ratios for O^+ and O_2^+ is normalized to 100. (b) PFI-PE spectrum (open circles) for O_2^+ ($b\,^4\Sigma_g^-$, $v^+=4$) in the energy range of 18.705–18.730 eV. The simulation based on the BOS model is shown in solid line (see the text). The marking of the $\Delta N=-2$, 0, and +2 (or *O*, *Q*, and *S*, respectively) rotational branches are also shown in (b). The numbers given in (b) are N'' values. The dashed line of (b) shows the population of O_2^+ ($b\,^4\Sigma_g^-$, $v^+=4$, $N^+<9$) estimated based on the BOS simulation.

resulting in $N^+=7$, 9, 11, 13, and 15 by 0.34, 1.50, 1.36, 1.21, and 1.41, respectively. The necessity to scale up the transitions for $N^+\geqslant 9$ by a factor of 1.2–1.5 is consistent with the conclusion that the rotational line strengths for the formation of $N^+\geqslant 9$ in the $O_2^+(b\,^4\Sigma_g^-, v^+=4)$ PFI-PE band are enhanced. No such enhancements are found in the $O_2^+(b\,^4\Sigma_g^-, v^+<4$ and $>5)$ PFI-PE bands. In the previous PFI-PE study of Hsu *et al.*,[53] the rotational intensity distribution observed in the $O_2^+(b\,^4\Sigma_g^-, v^+=5)$ PFI-PE band is also different from other PFI-PE bands. For this reason, Hsu *et al.* have interpreted the line strength enhancements for $O_2^+(b\,^4\Sigma_g^-, v^+=4, N^+\geqslant 9)$ as due to the crossing by the $d\,^4\Sigma_g^+$ potential curve in between the $O_2^+(b\,^4\Sigma_g^-, v^+=4$ and 5) levels.[64–67] The latter repulsive state is believed to be responsible for the predissociation of $O_2^+(b\,^4\Sigma_g^-, v^+\geqslant 4)$.

Two crossover points were observed in this breakdown diagram because the population of $Q(N^+>7)$ occurs on the low energy side and that of $S(N^+>7)$ lies on the high energy side of the $O_2^+(b\,^4\Sigma_g^-, v^+=4)$ band. The crossover point at 18.7207 eV locates between $Q(N^+=7$ and 9). The other crossover point at 18.7234 eV results from the population of $N^+(>7)$ level via the *S*-branch.

If $O^+(^4S)$ is formed by excited $O_2^+(b\,^4\Sigma_g^-, v^+\geqslant 4, N^+)$ prepared by the PFI of high-*n* O_2 Rydberg states $[O_2^*(n)]$ as indicated in process (3), we may not expect intensity enhancements for rotational levels ($N^+\geqslant 9$) disregarding any local perturbations due to low-*n* Rydberg states.

$$O_2+h\nu\rightarrow O_2^*(n)\rightarrow O_2^+(b\,^4\Sigma_g^-, v^+=4, N^+\geqslant 9)+e^- \rightarrow O^+(^4S)+O(^3P)+e^-. \quad (3)$$

Our previous lifetime measurements for $O_2^*(n)$ converging to dissociative[53,57,58,62] $O_2^+(b\,^4\Sigma_g^-, B\,^2\Sigma_g^-$, and $c\,^4\Sigma_u^-)$ states provide strong evidence indicating that prompt dissociation of $O_2^*(n)$ occurs to form $O^*(n')+O$ prior to PFI, where $O^*(n')$ represents an excited O atom in a high-n' Rydberg level. That is, the formation PFI-PEs are most likely resulted from PFI of $O^*(n')$. In this case, the $O^*(n')$ state converges to the $O^+(^4S)$ limit and the sequential steps for the PFI-PE formation is shown in process (4).

$$O_2+h\nu\rightarrow O_2^*(n)\rightarrow O^*(n')+O(^3P) \rightarrow O^+(^4S)+e^-+O(^3P). \quad (4)$$

If the lifetimes for $O^*(n')$ species formed above the dissociation threshold ($N^+\geqslant 9$) are longer than those for $O_2^*(n)$ below the dissociation threshold ($N\leqslant 7$), an increase in the PFI-PE intensity at $N^+\geqslant 9$ should be observed. A relative increase in rotational line strength for $N^+\geqslant 9$ levels lying about the dissociation limit can therefore be explained by this lifetime switching mechanism. We note that for the best fit, the levels resulting in $N^+=7$ had to be decreased. This may indicate that the lifetimes of $O_2^*(n)$ species converging to $N^+=7$ are shortened due to perturbation of low-*n* Rydberg states. We believe that the dissociation mechanism shown in processes (2) and (4) are valid for high-*n* Rydberg states converging to a dissociative ion core with a lifetime much shorter than the experimental time scale of ≈0.02–0.6 μs. The dissociative lifetimes for $O_2^+(b\,^4\Sigma_g^-, v^+\geqslant 4)$ have been measured to be <4 ns.

Once a good fit to the experimental PFI-PE is obtained, we were able to estimate the population for $N^+<9$. This population is shown in Fig. 10(a) by the dashed curve, revealing that the PFI-PE peak at 18.7220 eV corresponds predominantly to the formation of $O_2^+(b\,^4\Sigma_g^-, v^+=4, N^+<9)$. If we assume that the population of $O_2^+(b\,^4\Sigma_g^-, v^+=4, N^+\geqslant 9)$ led to prompt dissociation, the population for $O_2^+(b\,^4\Sigma_g^-, v^+=4, N^+<9)$ represents the intensity of O_2^+ observed in the PFI-PEPICO TOF spectrum. The calculated branching ratios for O^+ and O_2^+ are shown as the solid and dashed curves, respectively, in Fig. 10(b). We have also calculated the breakdown diagrams assuming that the dissociation thresholds for O^+ are at $N^+=7$ and 11. The comparison between the calculated and experimental breakdown curves for the assumed thresholds at $N^+=7$ and 11 are shown in Figs. 11(a) and 11(b), respectively. The respective populations for $O_2^+(b\,^4\Sigma_g^-, v^+=4, N^+<7)$ and $O_2^+(b\,^4\Sigma_g^-, v^+=4, N^+<11)$ along with the PFI-PE band for $O_2^+(b\,^4\Sigma_g^-, v^+=4)$ are depicted in Figs. 11(aa) and 11(bb). As pointed out above, the population of $O_2^+(b\,^4\Sigma_g^-, v^+=4, N^+<7)$ $[O_2^+(b\,^4\Sigma_g^-, v^+=4, N^+<11)]$ represents the intensity of O_2^+ for the assumed threshold of $N^+=7(N^+$

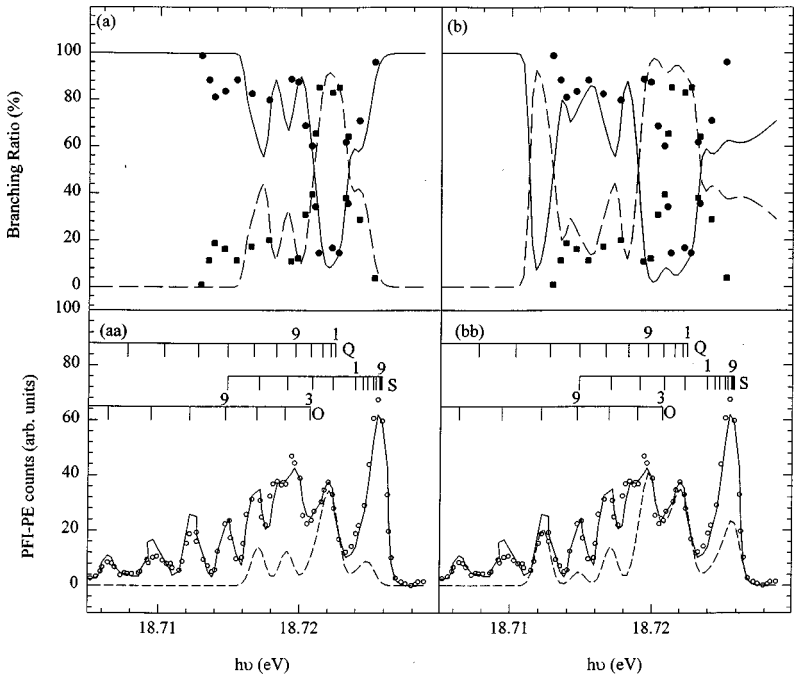

FIG. 11. Comparison between experimental breakdown diagram for the formation of $O^+(^4S)+O(^3P)$ from O_2 and that based on the assumed thresholds at $N^+=7$ and 11 are shown in (a) and (b), respectively. The solid circles represent the branching ratios of O^+ and the solid squares are those are O_2^+. At a given photon energy, the sum of the branching ratios for O^+ and O_2^+ is normalized to 100. The estimated populations (dashed curves) for O_2^+ ($b\,^4\Sigma_g^-$, $v^+=4$, $N^+<7$) and O_2^+ ($b\,^4\Sigma_g^-$, $v^+=4$, $N^+<11$) obtained based on the BOS simulation, along with the PFI-PE band (open circles) for O_2^+ ($b\,^4\Sigma_g^-$, $v^+=4$), are depicted in (aa) and (bb), respectively. The marking of the $\Delta N=-2$, 0, and +2 (or *O*, *Q*, and *S*, respectively) rotational branches are also shown in (aa) and (bb). The numbers given in (aa) and (bb) are N'' values.

$=11$). The simulation based on the assumed $N^+=11$ threshold produces a poor fit in the region 18.718–18.721 eV, while that for the $N^+=7$ threshold yields a poor fit in the region 18.712–18.716 eV. The assumed threshold of $N^+=9$ results in the best overall fit [Fig. 10(b)]. Since the optical resolution used in the branching ratio determination of Fig. 10(a) is different from that used in the PFI-PE measurement of Fig. 10(b), finite discrepancies between the simulated and measured branching ratios as shown in Fig. 10(b) are to be expected. The discrepancies can be attributed to the uncertainty of the determination of rotational population of O_2 using the BOS model. In addition to correctly predict the crossover points, the $N^+=9$ simulation also predicts the experimental observation that complete dissociation of O_2^+ occurs at energies >18.7253 and <18.7129 eV. Thus, the results of the present PFI-PEPICO study of O_2 support the previous conclusion[64–67] that the dissociation threshold for $O^+(^4S)+O(^3P)$ lies at $O_2^+(b\,^4\Sigma_g^-, v^+=4, N^+=9)$. This finding, together with the observation of the rotational intensity enhancement at $N^+\geqslant 9$ can be taken as strong support for the $O_2^*(n)/O^*(n')$ lifetime switching effect at the dissociation threshold.

An important aspect of a PEPICO experiment is the ability to determine the fragment KER of a prompt dissociation reaction.[12,24] Assuming that the mechanism for the O^+ formation proceeds by process (4), some information about the KER for the actual ion dissociation process may be lost because the formation of O^+ is mediated by the initial production of $O^*(n')$. If the delay of PFI with respect to the formation of $O^*(n')$ from $O_2^*(n)$ is short, the KER information may still be obtained with accuracy. In order to demonstrate this capability, we have measured the PFI-PEPICO TOF spectra for O^+ at energies 18.7171, 18.8501, 18.9717, and 19.0900 eV as shown in Figs. 12(a)–12(d), corresponding to the PFI-PE bands for $O_2^+(b\,^4\Sigma_g^-, v^+=4, 5, 6, \text{and } 7)$, respectively. The latter three energies are set at the respective highest intensity peak positions of the $v^+=5-7$ PFI-PE bands. These spectra were measured using a supersonically cooled O_2 sample and the two-bunch synchrotron radiation at the ALS.

Although the S/N ratios of these spectra are relatively poor, they reveal a nearly symmetric doublet structure. As-

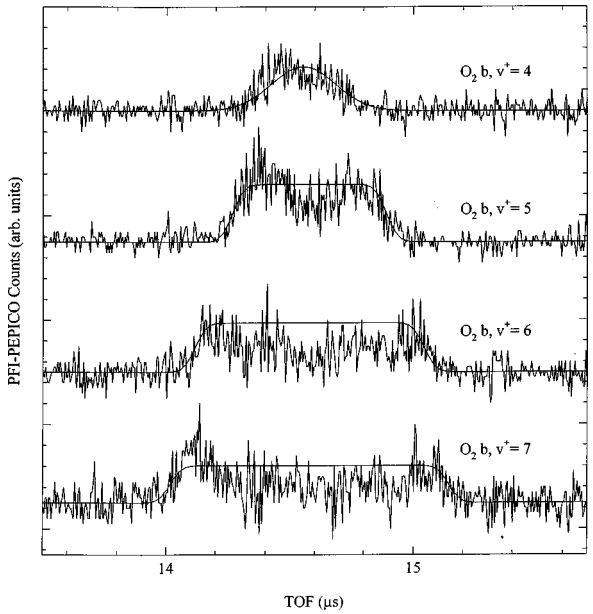

FIG. 12. Background subtracted PFI-PEPICO TOF spectra for O^+ obtained at energies 18.7171, 18.8501, 18.9717, and 19.0900 eV, corresponding to the PFI-PE bands for O_2^+ ($b\,^4\Sigma_g^-$, $v^+=4$, 5, 6, and 7), respectively. These spectra were measured using a supersonically cooled O_2 molecular beam and the two-bunch synchrotron radiation. The simulated TOF spectra (solid line) were obtained using an effective electric field of 4.5 V/cm. An O_2 temperature of $\approx$10 K was assumed in the simulation of the spectra measured at 18.8501, 18.9717, and 19.0900 eV. The simulated curve (solid line) at 18.7171 eV is obtained assuming an O_2 temperature of $\approx$100 K, indicating a higher contribution O^+ from thermal O_2 in the photoionization chamber.

suming a single kinetic energy release (KER) and an isotropic distribution, we expect to observe a rectangular TOF distribution in a static field experiment, whose full width Δt is predicted by the equation,[24,71]

$$\Delta t = \sqrt{\frac{8mE_{c.m.}}{(qF)^2}}. \tag{5}$$

Here, $E_{c.m.}$ is the center-of-mass kinetic energy of the ion with a mass (m), F is the electric field at the PI/PEX region, and q is the elementary charge. The Δt value of these TOF peaks simply corresponds to the turn around time of the most energetic O^+ ion moving away from the TOF ion detector. In the dissociation reaction of O_2^+ into $O^+ + O$, the entire excess energy must be released into the kinetic energy of the fragments, suggesting a single KER value disregarding the spin-orbit splitting of $O(^3P)$. The concave peak profile observed is indicative of the discrimination in the collection efficiency of energetic ions produced with velocity components perpendicular to the ion TOF axis. The Δt value is found to increase as v^+ is varied from 5 to 7, consistent with the expected increase in KER. The KER of the dissociation process can be obtained from the measured Δt value provided that the effective electric field at the PI/PEX region is known. Since the ion-extraction field pulse is only on for <160 ns and the O^+ ions remain in the PI/PEX region at the end of the field pulse, it is difficult to estimate the effective field at the PI/PEX region. This is especially the case when considering finite imperfections, such as ringing, of the applied electric field pulse for ion extraction.

We have satisfactorily simulated the TOF distributions observed in Figs. 12(a)–12(d) using an effective electric field of 4.5 V/cm. The simulated spectra (solid lines) of Figs. 12(b)–12(d) are obtained by assuming an O_2 temperature of $\approx$10 K. The simulated curve (solid line) of Fig. 12(a) is obtained assuming an O_2 temperature of $\approx$100 K, indicating a higher contribution of O^+ from thermal O_2 in the photoionization chamber. As pointed out above, the thermal O_2 background is estimated to be $\approx$15%. The higher thermal O_2 contribution associated with the $O_2^+(b\,^4\Sigma_g^-, v^+=4)$ spectrum can be accounted for by the fact that at 18.7171 eV the thermal PFI-PE spectrum dominates. The higher thermal contribution is also due partly to the lifetime switching effect, i.e., the enhancement of line strengths for rotational levels $N^+ \geqslant 9$ as manifested in the PFI-PE band for $O_2^+(b\,^4\Sigma_g^-, v^+=4)$. The dissociation arising from thermal O_2 molecules will lead to a distribution of kinetic energies for O^+. In this case, the TOF distribution can be obtained as the sum of many rectangular basis functions with appropriate weighting determined by the transformation from the energy to the TOF domain. The simulated TOF spectra for O^+ from $O_2^+(b\,^4\Sigma_g^-, v^+=4-7)$ shown in Figs. 12(a)–12(d) are in reasonably good agreement with the PFI-PEPICO TOF spectra.

The known KERs for the dissociation of $O_2^+(b\,^4\Sigma_g^-, v^+=4-7)$ are plotted versus the simulated KERs in Fig. 13. The simulated and experimental KERs are in good accord. Due to the difficulty in assessing the thermal background contribution, we assign an uncertainty of 39 meV (the average translational energy for thermal O_2 molecules) for the simulated KER values.

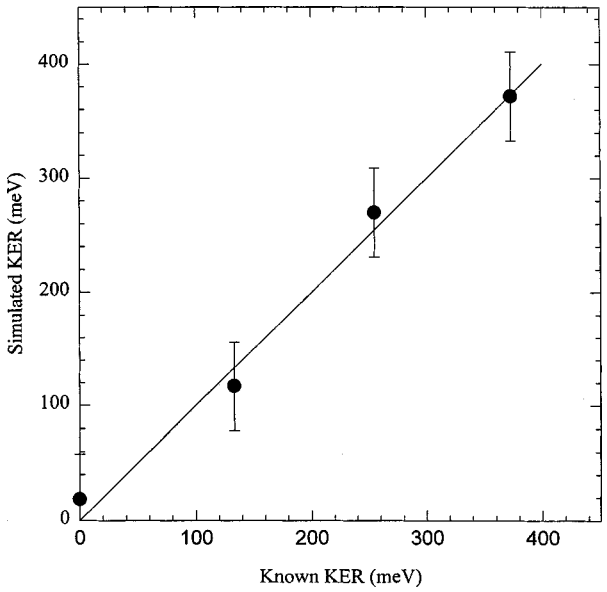

FIG. 13. Known KER for the dissociation of O_2^+ ($b\,^4\Sigma_g^-$, $v^+=4-7$) plotted vs the simulated KER. Due to the difficulty in assessing the thermal background contribution, an uncertainty of 39 meV (the average translational energy for thermal O_2 molecules) is assigned for the simulated KER values.

IV. FURTHER ADVANCES

A major disadvantage of the PFI-PEPICO scheme described in Sec. II C is that the use of a relatively high pulsed electric field limits the achievable PFI-PE or PFI-PEPICO resolution to $\approx$1.0 meV. One way of improving this is to use a shaped pulse, which consists of a low field (<1 V/cm, duration $\approx$20–40 ns) for PFI immediately followed by a higher field pulse (>7 V/cm, duration $\approx$150 ns) for ion extraction. We note that since the ion-extraction pulse has a finite overlap with VUV light bunches, PFI-PEs will also be generated. However, PFI-PEs produced by the low and high pulses should arrive in two time windows. By collecting only PFI-PEs from the low field pulse, the resolution is expected to be higher than that obtained in the scheme of Sec. II C, where a 7 V/cm height pulsed field is used for PFI. In this shaped pulse scheme, an important experimental consideration is that the PFI-PEs formed by PFI due to the low field pulse must exit the PI/PEX region prior to the employment of the high field pulse. As the PFI-PEs exit the PI/PEX region and enter the electron TOF spectrometer, they are shielded from the high field pulse by the grid located at the aperture of lens E1 (see Fig. 1). As a result, the TOF of the PFI-PEs formed by the low field pulse is not disturbed by the high field pulse for ion extraction.

We have just fabricated the necessary pulser and electronics for this shaped pulse scheme. The advantage of this scheme in yielding higher PFI-PEPICO resolution is shown Fig. 14, where the PFI-PE (open circles) and PFI-PEPICO (solid circles) bands for $Ar^+(^2P_{3/2,1/2})$ are compared. These spectra were obtained using a 0.5 V/cm low field pulse

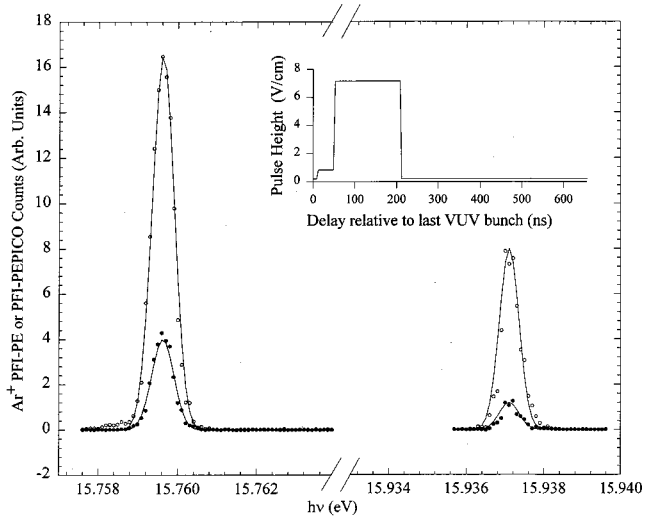

FIG. 14. Comparison of the PFI-PE (open circles) and PFI-PEPICO (solid circles) bands for $Ar^+(^2P_{3/2,1/2})$ obtained using the shaped pulse coincidence scheme. The shaped pulse is shown in the inset. It consists of a 0.5 V/cm low field pulse (duration=40 ns) followed by a 7 V/cm high field pulse (duration=150 ns). The Gaussian fit to these bands yields a resolution of 0.6 meV (FWHM) for both the PFI-PE and PFI-PEPICO bands.

(duration=40 ns) followed by a 7 V/cm high field pulse (duration=150 ns). The pulse shape used is shown in the inset of Fig. 14. The Gaussian fit to the $Ar^+(^2P_{3/2})$ and $Ar^+(^2P_{1/2})$ bands gives experimental resolutions of 0.6 and 0.5 meV (FWHM), respectively. The slightly higher resolution for the $Ar^+(^2P_{1/2})$ band is most likely caused by a shorter lifetime of the Rydberg states converging to this ionization limit. We note that PFI-PEPICO intensity is about 25% of the PFI-PE intensity, indicating good collection efficiencies for both PFI-PEs and PFI ions. The shaped pulse basically solves the dilemma of achieving a high photoelectron resolution (requires a low electric field pulse) and a high ion transmission (requires a high electric field pulse). We believe that this new synchrotron-based PFI-PEPICO method will have a significant impact to thermochemistry and unimolecular and bimolecular reaction dynamics studies of cations.

ACKNOWLEDGMENTS

This work was supported by the Director, Office of Energy Research, Office of Basic Energy Sciences, Chemical Science Division of the U.S. Department of Energy under Contract No. W-7405-Eng-82 for the Ames Laboratory and Contract No. DE-AC03-76SF00098 for the Lawrence Berkeley National Laboratory. K.M.W. and M.M. acknowledge financial supported by the Deutsche Forschungsgemeinschaft. CYN acknowledges the support of the Alexander von Humboldt Senior Scientist Award. Y.S. is the recipient of the 1999 Wall Fellowship at Iowa State University.

[1] H. M. Rosenstock, M. K. Draxl, B. W. Steiner, and J. T. Herron, J. Phys. Chem. Ref. Data Suppl. **6**, 1 (1977).
[2] S. G. Lias, J. E. Bartmess, J. L. Holmes, R. D. Levin, and W. G. Mallard, J. Phys. Chem. Ref. Data Suppl. **17**, 1 (1988).
[3] D. W. Turner, C. Baker, A. D. Baker, and C. R. Brundle, *Molecular Photoelectron Spectroscopy* (Wiley, London, 1970).
[4] J. W. Rabalais, *Principle of Ultraviolet Photoelectron Spectroscopy* (Wiley, New York, 1977).
[5] K. Kimura, S. Katsumata, Y. Achibi, T. Yamazaki, and S. Iwata, *Handbook of Hel Photoelectron Spectra of Fundamental Organic Molecules* (Halsted Press, Tokyo, 1981).
[6] E. v. Puttkammer, Z. Naturforsch. A **25**, 1062 (1970).
[7] D. Villarejo, R. R. Herm, and M. G. Inghram, J. Chem. Phys. **46**, 4495 (1967).
[8] W. B. Peatman, T. B. Borne, and E. W. Schlag, Chem. Phys. Lett. **3**, 492 (1969).
[9] T. Baer, W. B. Peatman, and E. W. Schlag, Chem. Phys. Lett. **4**, 243 (1969).
[10] R. Spohr, P. M. Guyon, W. A. Chupka, and J. Berkowitz, Rev. Sci. Instrum. **42**, 1872 (1971).
[11] P.-M. Guyon and T. Baer, in *High Resolution Laser Photoionization and Photoelectron Studies*, edited by I. Powis, T. Baer, and C. Y. Ng, Wiley Series in Ion Chemistry and Physics (Wiley, Chichester, 1995), Chap. 1.
[12] T. Baer, in *Gas Phase Ion Chemistry*, edited by M. T. Bowers (Academic, New York, 1979), Vol. 1, p. 153.
[13] T. Baer, Adv. Chem. Phys. **64**, 111 (1986).
[14] T. Baer, J. Booze, and K.-M. Weitzel, in *Vacuum Ultraviolet Photoionization and Photodissociation of Molecules and Clusters*, edited by C. Y. Ng (World Scientific, Singapore, 1991), p. 259.
[15] H. M. Rosenstock, R. Buff, M. A. A. Ferreira, S. G. Lias, A. C. Parr, R. Stockbauer, and J. L. Holmes, J. Am. Chem. Soc. **104**, 2337 (1982).
[16] J. P. Gilman, T. Hsieh, and G. G. Meisels, J. Chem. Phys. **78**, 3767 (1983).
[17] T. Nishimura, P. R. Das, and G. G. Meisels, J. Chem. Phys. **84**, 6190 (1986).
[18] T. Baer, J. C. Morrow, J. D. Shao, and S. Olesik, J. Am. Chem. Soc. **110**, 5633 (1988).
[19] K. Norwood, A. Ali, G. D. Flesch, and C. Y. Ng, J. Am. Chem. Soc. **112**, 7502 (1990).
[20] K. Norwood and C. Y. Ng, J. Chem. Phys. **93**, 6440 (1990).
[21] O. Dutuit, T. Baer, C. Metayer, and J. Lemaire, Int. J. Mass Spectrom. Ion Processes **110**, 67 (1991).
[22] K. M. Weitzel, J. Mahnert, and M. Penno, Chem. Phys. Lett. **224**, 371 (1994).
[23] F. Güthe and K.-M. Weitzel, Ber. Bunsenges. Phys. Chem. **104**, 484 (1997).
[24] M. Evans, C. Y. Ng, C.-W. Hsu, and P. Heimann, J. Chem. Phys. **106**, 978 (1997).
[25] J. Mähnert, F. Güthe, and K.-M. Weitzel, Ber. Bunsenges. Phys. Chem. **100**, 1899 (1996).
[26] K. Norwood, J. H. Guo, G. Luo, and C. Y. Ng, J. Chem. Phys. **90**, 6026 (1989).
[27] K. Norwood, A. Ali, and C. Y. Ng, J. Chem. Phys. **95**, 8029 (1991).
[28] K. Norwood and C. Y. Ng, Chem. Phys. Lett. **156**, 145 (1989).
[29] C. Y. Ng, in *Vacuum Ultraviolet Photoionization and Photodissociation of Molecules and Clusters*, edited by C. Y. Ng (World Scientific, Singapore, 1991), pp. 169–257.
[30] W. Kamke, in *Cluster Ions*, edited by C. Y. Ng, T. Baer, and I. Powis (Wiley, Chichester, 1993), p. 1.
[31] K. Mitsuke and K. Ohno, J. Phys. Chem. **93**, 501 (1989).
[32] J. A. Booze and T. Baer, J. Chem. Phys. **96**, 5541 (1992).
[33] J. Mahnert, H. Baumgärtel, and K.-M. Weitzel, J. Chem. Phys. **103**, 7016–7024 (1995).
[34] Y. Morioka, T. Tanaka, H. Yoshii, and T. Hayaishi, J. Chem. Phys. **109**, 1324 (1998).
[35] P. M. Guyon, T. R. Govers, and T. Baer, Z. Phys. D **4**, 89 (1986).
[36] P. M. Guyon, T. Baer, S. K. Cole, and T. R. Govers, Chem. Phys. **119**, 145 (1988).
[37] C. Y. Ng, in *Techniques for the Study of Ion-Molecule Reactions*, edited by J. M. Farrar and W. H. Saunders, Jr. (Wiley, New York, 1988), p. 417.
[38] T. Baer, L. Squires, and A. S. Werner, Chem. Phys. **6**, 325 (1974).
[39] I. Koyano and K. Tanaka, in *State-Selected and State-to-State Ion-Molecule Reaction Dynamics I: Experiment*, edited by C. Y. Ng and M. Baer (Wiley, New York, 1992); Adv. Chem. Phys. **82**, 263 (1992).
[40] E. Waterstradt, R. Jung, H.-J. Deitrich, and K. Mullér-Dethlefs, Rev. Sci. Instrum. **64**, 3104 (1993).
[41] R. I. Hall, A. McConkey, K. Ellis, G. Dawber, L. Avaldi, M. A. MacDonald, and G. C. King, Meas. Sci. Technol. **3**, 316 (1992).
[42] Y. Lu, Y. Morioka, T. Matsui, T. Tanaka, H. Hoshii, R. I. Hall, T. Hayaishi, and K. Ito, J. Chem. Phys. **102**, 1553 (1995).

[43] Y. Morioka, Y. Lu, T. Matsui, T. Tanaka, H. Yoshii, T. Hayaishi, and R. I. Hall, J. Chem. Phys. **104**, 9357 (1996).
[44] *High Resolution Laser Photoionization and Photoelectron Studies*, edited by I. Powis, T. Baer and C. Y. Ng, Wiley Series in Ion Chemistry and Phsics (Wiley, Chichester, 1995).
[45] G. Reiser, W. Habenicht, K. Muller-Dethlefs, and E. W. Schlag, Chem. Phys. Lett. **152**, 119 (1988).
[46] K. Muller-Dethlefs, M. Sander, and E. W. Schlag, Z. Naturforsch. Teil A **39**, 1089 (1984).
[47] K.-M. Weitzel and F. Güthe, Chem. Phys. Lett. **251**, 295 (1996).
[48] C.-W. Hsu, M. Evans, P. Heimann, K. T. Lu, and C. Y. Ng, J. Chem. Phys. **105**, 3950 (1996).
[49] C.-W. Hsu, M. Evans, C. Y. Ng, and P. Heimann, Rev. Sci. Instrum. **68**, 1694 (1997).
[50] R. C. Shiell, M. Evans, S. Stimson, C.-W. Hsu, C. Y. Ng, and J. W. Hepburn, Phys. Rev. Lett. **80**, 472 (1998).
[51] C.-H. Hsu, P. Heimann, M. Evans, S. Stimson, and C. Y. Ng, Chem. Phys. **231**, 121 (1998).
[52] S. Stimson, Y.-J. Chen, M. Evans, C.-L. Liao, C. Y. Ng, C.-W. Hsu, and P. Heimann, Chem. Phys. Lett. **289**, 507 (1998).
[53] S. Stimson, M. Evans, C. Y. Ng, C. Destandau, G. Chambaud, P. Rosmus, C.-W. Hsu, and P. Heimann, J. Chem. Phys. **108**, 6205 (1998).
[54] M. Evans, S. Stimson, C. Y. Ng, and C.-W. Hsu, J. Chem. Phys. **109**, 1285 (1998).
[55] C.-W. Hsu, M. Evans, S. Stimson, C. Y. Ng, and G. K. Jarvis, J. Chem. Phys. **110**, 315 (1999).
[56] G. K. Jarvis, Y. Song, and C. Y. Ng, Rev. Sci. Instrum. **70**, 2615 (1999).
[57] P. Heimann, M. Koike, C.-W. Hsu, M. Evans, K. T. Lu, C. Y. Ng, A. Suits, and Y. T. Lee, Rev. Sci. Instrum. **68**, 1945 (1997).
[58] C. Y. Ng, in *Photroionization and Photodetachment*, edited by C. Y. Ng, Adv. Ser. Phys. Chem. (World Scientific, Singapore, 1999), Vol. 10A (in press).
[59] A. Tabché-Fouhailé, I. Nenner, P. M. Guyon, and J. Delwiche, J. Chem. Phys. **75**, 1129 (1981).
[60] P. C. Cosby, J.-B. Ozenne, J. T. Moseley, and D. L. Albritton, J. Mol. Spectrosc. **79**, 203 (1980).
[61] J. T. Moseley, P. C. Cosby, J.-B. Ozenne, and J. Durup, J. Chem. Phys. **70**, 1474 (1979).
[62] J. C. Hansen, J. T. Moseley, A. L. Roche, and P. C. Cosby, J. Chem. Phys. **77**, 1206 (1982).
[63] H. Helm, P. C. Cosby, and D. L. Huestis, J. Chem. Phys. **73**, 2629 (1980).
[64] W. C. Wiley and I. H. McLaren, Rev. Sci. Instrum. **26**, 1150 (1955).
[65] W. A. Chupka, J. Chem. Phys. **98**, 4520 (1993).
[66] J. Jortner and M. Bixon, J. Chem. Phys. **99**, 3133 (1995).
[67] T. F. Gallagher, *Rydberg Atoms* (Cambridge University Press, Cambridge, 1994).
[68] M. Penno, A. Holzwarth, and K.-M. Weitzel, Mol. Phys. (in press).
[69] K.-M. Weitzel, M. Malow, G. K. Jarvis, T. Baer, Y. Song, and C. Y. Ng, J. Chem. Phys. (submitted).
[70] G. Jarvis, K.-M. Weitzel, M. Marcus, T. Baer, Y. Song, and C. Y. Ng, Phys. Chem. Chem. Phys. (submitted).
[71] J. L. Franklin, P. M. Hierl, and D. A. Whan, J. Chem. Phys. **47**, 3148 (1967).